Journal of Materials Chemistry A

Accepted Manuscript

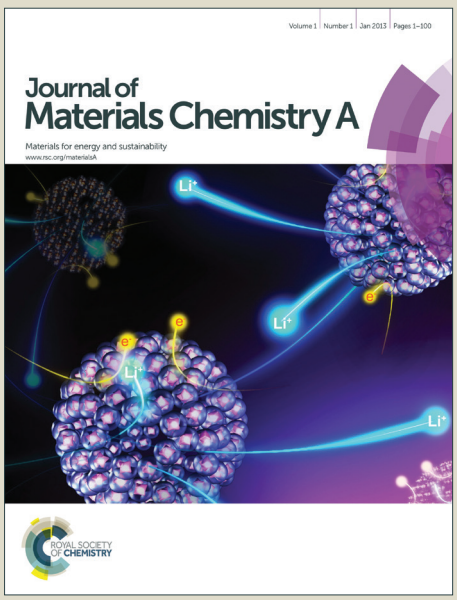

ROYAL SOCIETY OF CHEMISTRY

www.rsc.org/materialsA

Hydrophilization of Polysulfone Membranes Using a Binary Graft Copolymer

Yang Yang,[1,2,3] Lei Miao,[1,2,3] Jiwen Hu,[*,1,2,3] Guojun Liu,[*,1,2,4] Yuanyuan Tu,[1,2] Shudong Lin,[1,2] Feng Liu,[1,2] Fei Li,[1,2,3] Yan Wu,[1,2,3] Ganwei Zhang,[1,2] and Hailiang Zou[1,2]

[1]Guangzhou Institute of Chemistry, Chinese Academy of Sciences, Guangzhou, P. R. China, 510650; [2]Key Laboratory of Cellulose and Lignocellulosics Chemistry, Chinese Academy of Sciences, P. R .China, 510650; [3] University of Chinese Academy of Science, Beijing, P.R. China, 100049; [4]Department of Chemistry, Queen's University, 90 Bader Lane, Kingston, Ontario, K7L 3N6, Canada

Abstract: An amphiphilic binary graft copolymer polysulfone-*graft*-[poly(methyl methacrylate)-*random*-poly(acrylic acid)], PSf-*g*-(PMMA-*r*-PAA), was synthesized via a combination of atom transfer radical polymerization (ATRP) and click chemistry. This copolymer and polysulfone (PSf) were used to prepare porous membranes through the phase inversion method, which involved dissolving the polymers in a common solvent *N*-methyl pyrolidone (NMP), casting the solution onto a glass plate to obtain a film, and subsequently immersing this film into a coagulant (a mixture of dimethylformamide and water at a given pH). The surfaces of the membrane and its pore walls were covered by the copolymer, and these surfaces were enriched with PAA domains due to the immiscibility between PAA and PSf and the miscibility between PMMA and PSf. More specifically, while the hydrophobic PMMA component served as an anchor to fix the graft copolymer onto the PSf bulk substrate,

* Corresponding author, email: hjw@gic.ac.cn, fax: 86-20-85232307

the hydrophilic PAA component assembled and became exposed at the surfaces of the membrane and the pore walls. Factors influencing this surface AA concentration or carboxyl group content (CGC) enrichment and the surface and pore morphologies of the membranes have included the ratio between the amount of the copolymer and PSf in the mixture, the solvent quality of the coagulant for PSf, and the pH of the coagulant. These factors have been systematically adjusted to optimize the hydrophilization of the PSf membrane and the resultant membranes have been characterized by water contact angle (WCA) measurements, scanning electron microscopy (SEM), atomic force microscopy (AFM), and via X-ray photoelectron spectroscopy (XPS). Optimization of the phase inversion process yielded membranes with nearly complete surface coverage by PAA, even when the graft copolymer represented only 8 wt% of the membrane's composition. The hydrophilized membranes exhibited increased water flux and even pH-responsive water flow without adversely affecting their mechanical properties. In addition, these hydrophilic membranes exhibited long-term stability. Therefore, this novel binary amphipilic graft copolymer-based approach for membrane modification may be of commercial value.

Keywords: amphiphilic binary graft copolymers, polysulfone (PSf), membranes, surface segregation, phase inversion

1. Introduction

Membranes are widely used for gas or liquid separation.[1-5] The surface hydrophilicity of a porous membrane improves its biocompatibility[6, 7] and facilitates its permeation by polar liquids[8] and the binding of polar reagents.[9] Further, surface hydrophilization protects membranes against bio-fouling, which decreases the permeation flux and selectivity of membranes.[10-13] Therefore, the hydrophilization of the surfaces of hydrophobic membranes has been an important area of membrane research.

There are currently only a few commercial membranes made from hydrophilic polymers including poly(vinyl alcohol), cellulose or its derivatives, and polyacrylonitrile,[14-16] since hydrophilic polymers do not necessarily have the desired thermal and dimensional stability or chemical resistance.[12, 17] On the other hand, many hydrophobic thermoplastics such as polyimide, polysulfone (PSf), polypropylene (PP), polyvinylidene fluoride (PVDF), etc[12, 18, 19] have desirable mechanical and chemical properties. Therefore, the hydrophilization of membranes made from these polymers has been a topic of many recent studies.[12, 20-24] Two approaches have been adopted so far to hydrophilize polymer membranes.[23, 25] The first approach has involved the surface modification of pre-made membranes. Specific strategies employed have included physical coating[26] or surface grafting of hydrophilic species onto membrane surfaces as well as the plasma-treatment of membrane surfaces to generate polar species.[27, 28] A major disadvantage of this approach is that the pore sizes decrease after the deposition or grafting of a new

species onto the pore walls.[11, 12]

The other general strategy involves membrane formation from a mixture consisting of a hydrophobic polymer along with a hydrophilic additive. Using this approach, membranes have been prepared from *β*-cyclodextrin/PSf,[29, 30] cellulose diacetate/PSf,[31] polyaniline (PANi)/PSf,[32] P(MMA-*r*-POEM)/PVDF[33] or even hydrophilic inorganic nanoparticles with hydrophobic polymers such as Fe_3O_4/PSf,[34] SiO_2/PVDF,[35] and zirconia/PSf.[36] Due to the immiscibility between the hydrophilic components and the hydrophobic polymers, the interfacial bonding between the different components can be an issue for some of the reported membrane formulations. The interfacial bonding can be improved with the use of an amphiphilic random or block copolymers which bear hydrophobic components that readily mixes with the matrix polymer and hydrophilic components that render the desired hydrophilicity.[12, 13, 20, 21, 37]

We imagined that the interfacial bonding would be further improved if an amphiphilic binary graft copolymer was used as a hydrophilic additive during membrane formation. The graft copolymer could be PA-*g*-(PB-*r*-PC), where PA, PB, and PC denoted the linear backbone chain, the hydrophobic side chains, and the hydrophilic side chains, respectively (Scheme 1a). We further fancied that a solution could be cast as a film onto a glass plate from this graft copolymer together with a bulk hydrophobic polymer that was compatible with PB. The immersion of this solution film into a coagulation bath would cause phase inversion to take place and result in a porous film. The graft copolymer should segregate more readily than a

random copolymer P(B-*r*-C) or a block copolymer PB-*b*-PC because of the larger excluded volume of the graft copolymer.[24] The PB chains would be more securely anchored onto the membrane surface and membrane pore walls because the removal or detachment of a PA-*g*-(PB-*r*-PC) chain would require the coordinated motion or co-operative motions of all the PB chains as well as the PA backbone.[13, 38] Therefore, it is anticipated that the introduction of the PB chains of PA-*g*-(PB-*r*-PC) onto a bulk membrane will provide the membrane with more durable hydrophilicity than would be provided by the incorporation of a random copolymer, block copolymer, or graft copolymerwith only hydrophilic side chains such as P(B-*r*-C) PB-*b*-PC, or PA-*g*-PC, respectively.[37]

As a proof of concept, we have prepared the amphiphilic binary graft copolymer polysulfone-*graft*-[poly(methyl methacrylate)-*random*-poly(acrylic acid)] (denoted as PSf-*g*-(PMMA-*r*-PAA) or ABP, Scheme 1b) and used this graft copolymer to prepare membranes with PSf. PSf was chosen as the membrane matrix material because commercial PSf membranes have been widely used in gas separation,[39] pervaporation,[40] hemodialysis,[41] nano/ultra-filtration,[42] and other applications.[43] PMMA was used as one type of grafts because of its compatibility with PSf,[44] while PAA was chosen for its pH sensitivity and its ability to form an ionic and hydrophilic species.[20, 21]

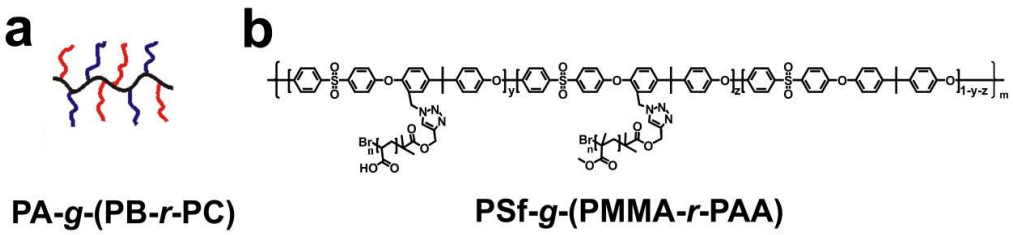

Scheme 1. Illustration of an amphiphilic binary graft copolymer (a) and the structure of PSf-*g*-(PMMA-*r*-PAA), which is also denoted as ABP (b).

While amphiphilic copolymers such as linear random copolymers,[45] linear block copolymers,[21, 24] and graft copolymers bearing only hydrophilic side chains[13, 46-48] have been used to hydrophilize porous polymer membranes, the use of binary graft copolymers to hydrophilize porous membranes is a novel strategy. Aside from this graft copolymer-based approach toward functional materials reported here, we have also recently reported on the use of graft copolymers in the preparation of nanoemulsions and nanocapsules[49, 50] as well as the use of pH-responsive nanoemulsions for drug release applications.[51]

2. Experimental methods

2.1 Materials and reagents

Polysulfone (PSf, Udel®P1700 NT LCD, M_n = 39,000 g/mol) was supplied by Solvay Specialty Polymers. Meanwhile, Paraformaldehyde (96%), tin(IV)chloride ($SnCl_4$) (99%), chlorotrimethylsilane ($(CH_3)_3SiCl$, 99%), CuBr (98%), disodium ethylenediamine tetraacetate (EDTA, 99%), *tert*-butyl methacrylate (tBA, 99%),

methyl methacrylate (MMA, 99%), sodium azide (NaN_3, 99%), 4,4′-dinonyl-2,2′-dipyridyl (dNbpy, 97%), tetrabutylammonium fluoride (TBAF, 98%), *N,N,N′,N′,N″*-pentamethyldiethylenetriamine (PMDETA, 98%), methanol (CH_3OH, 99%), dioxane (99%), toluene (99%), 1-methyl-2-pyrrolidinone (NMP, 99%), dichloromethane (DCM, 99%), *N,N*-dimethylformamide (DMF, 99%), diethyl ether (99%), thionin acetate (THA, 99%), and diphenyl ether (99%) were purchased from Aladdin Reagent of China. PSf was purified via dissolution into THF and precipitation from a mixture of methanol/water at 1/1 (v/v) before it was dried at 50 ^oC under vacuum for 48 h. MMA and tBA were purified by washing these reagents thrice with equal amounts of an aqueous 10 wt% NaOH solution before they were washed with water until the water tested was neutral. They were subsequently dried over anhydrous sodium sulfate and then distilled under reduced pressure prior to use. DCM was refluxed over CaH_2 overnight and distilled prior to use. Diphenyl ether, diethyl ether, dioxane and toluene were refluxed over a sodium wire and distilled before use. DMF was dried over anhydrous magnesium sulfate for three days and distilled prior to use. CuBr, Paraformaldehyde, $SnCl_4$, $(CH_3)_3SiCl$, EDTA, NaN_3, TBAF, dNbpy, PMDETA THA, and NMP were all used as received without further purification. The initiator 3-(trimethylsilyl)-propargyl 2-bromoisobutyrate was synthesized according to a previously reported procedure.[50, 52] All other reagents and solvents were used as received unless otherwise specified.

2.2 Preparation of P(Sf-CH_2N_3)

Synthesis of P(Sf-CH_2Cl). The chloromethylation of PSf was performed

according to previously reported procedures.[13] In a typical preparation, 10.00 g (22.5 mmol) of PSf was dissolved in 350 mL of chloroform under stirring. Subsequently, 6.70 g (225 mmol) of paraformaldehyde, 0.17 mL (1.50 mmol) of $SnCl_4$, and 28.60 mL (225 mmol) of $(CH_3)_3SiCl$ were added to the PSf solution. The reaction mixture was stirred at 50 ^oC for three days, and concentrated under reduced pressure via rotary evaporation to ~50 mL before it was precipitated out over 500 mL of methanol. The precipitate was collected by filtration and subsequently dissolved in chloroform and re-precipitated out over methanol. This precipitate was subsequently dried under vacuum overnight at 24 ^oC for 48 h, yielding 10.05 g of P(Sf-CH_2Cl) as a white powder. ^1H NMR characterization revealed that the degree of substitution (DS), which represented the percentage of chloromethylation per repeat unit of the PSf chain, was 0.6.

Synthesis of P(Sf-CH_2N_3). P(Sf-CH_2N_3) was synthesized by reacting P(Sf-CH_2Cl) with NaN_3 according to a previously reported procedure, along with some modifications.[13] In summary, P(Sf-CH_2Cl) (2.0 g, or 4.2 mmol) was fully dissolved into 60 mL of dry DMF before the addition of NaN_3 (0.82 g, or 12.6 mmol). After the reaction mixture was stirred for 24 h at 60 ^oC, the reaction mixture was concentrated and precipitated out over a mixture of methanol/water at 4/1 (v/v). The precipitates were collected and dried under vacuum overnight at 25 ^oC for 48 h, yielding 2.0 g of P(Sf-CH_2N_3) as a white powder. The DS, which in this case represented the percentage of azidomethylation per repeat unit of the PSf chain, was found to be 0.6 according to ^1H NMR analysis.

2.3 Preparation of PMMA-C≡CH and PtBA-C≡CH

Synthesis of PMMA-C≡CH. PMMA-C≡CH was synthesized in two steps. Firstly, PMMA-C≡CSi$(CH_3)_3$ was prepared via ATRP by using 3-(trimethylsilyl)-propargyl 2-bromoisobutyrate as the initiator and CuBr/dNbpy as the catalyst. In summary, CuBr (0.07 g, 0.50 mmol), MMA (10.0 g, 100 mmol), diphenyl ether (10.0 mL) and dNbpy (0.41 g, 1.0 mmol) were added into a dry Schlenk flask. This mixture was deoxygenated with argon by performing four freeze-pump-thaw cycles. 3-(Trimethylsilyl)-propargyl 2-bromoisobutyrate (0.28 g, 1.0 mmol) was then added via a degassed syringe under an argon atmosphere. The Schlenk flask was transferred into a pre-heated oil bath at 90 ^oC and stirred for 1 h. The reaction was stopped by freezing the flask with liquid nitrogen before introducing air inside the flask, causing the color of the reaction mixture to change from deep green to blue. The mixture was then diluted with 5 mL of CH_2Cl_2 and passed through an activated neutral alumina column to remove the catalyst. After the solvents were removed under reduced pressure via rotary evaporation at 60 ^oC, the residue (~2.0 mL) was added into 20 mL of n-hexane to precipitate the polymer. Finally, the obtained product (PMMA-C≡CSi$(CH_3)_3$) was dried under vacuum at 60 ^oC for 24 h, yielding 4.94 g of the product as a white powder in a 49.4% yield.

In the second step, the trimethylsilyl protecting group of PMMA-C≡CSi$(CH_3)_3$ was removed via hydrolysis in the presence of tetrabutylammonium fluoride, which served as a catalyst. In a typical procedure, PMMA-C≡CSi$(CH_3)_3$ (4.0 g) was dissolved in CH_2Cl_2 (30.0 mL) before the addition of 2.1 g (8.0 mmol) of

tetrabutylammonium fluoride. The reaction mixture was stirred at room temperature for 72 h. The obtained solution was washed with water twice (2 x 50 mL) to remove residual salts before most of the solvent was removed under reduced pressure. The obtained product was dried under vacuum for three days, generating 3.5 g of PMMA-C≡CH as a white powder in a yield of 87.5%. The complete removal of trimethylsilyl protecting group was demonstrated via ^{1}H NMR analysis.

Synthesis of PtBA-C≡CH. PtBA-C≡CH was synthesized analogously by two steps. The intermediate product PtBA-C≡CSi$(CH_3)_3$ was obtained in a 52.2% yield, while the final product PtBA-C≡CH was obtained in an 89.1% yield.

2.4 Preparation of PSf-*g*-(PMMA-*r*-PAA)

PSf-*g*-(PMMA-*r*-PtBA) was prepared by grafting PMMA-C≡CH and PtBA-C≡CH chains onto a P(Sf-CH_2N_3) backbone via click chemistry.[13] In a typical procedure, P(Sf-CH_2N_3) (1.0 g, containing 1.3 mmol of -N_3 groups), PMMA-C≡CH (0.66 g, 0.13 mmol), PtBA-C≡CH (0.84 g, 0.13 mmol) and a catalyst (CuBr, 1.30 mmol) were added into a flask and dissolved in 60 mL of DMF. The flask was deoxygenated by subjecting it to three freeze-pump-thaw cycles. PMDETA (0.22 g, 1.30 mmol) was then added by a degassed syringe. After the reaction proceeded at 25 ^{o}C for 72 h, the mixture was diluted with THF and then passed through a neutral alumina column to remove the metal salt. The reaction mixture was concentrated and precipitated out over water. The precipitate was collected and dried under vacuum at room temperature, generating 2.21 g of PSf-*g*-(PMMA-*r*-PtBA) as a white

powder in an 88.5% yield.

PSf-*g*-(PMMA-*r*-PAA) was prepared through the hydrolysis of PSf-*g*-(PMMA-*r*-PtBA) with concentrated HCl.[53] PtBA was converted to PAA by adding PSf-*g*-(PMMA-*r*-PtBA) (1.50 g) to a round bottom flask containing 60 mL of dioxane and 6 mL of concentrated HCl (37 wt%). The solution was stirred and heated at 100 ^{o}C. After the reaction had proceeded for 5 h, the solution was cooled down and a portion of the excess reagent (~50 mL) was removed via evaporation under vacuum. Subsequently, the mixture was precipitated out over 200 mL of H_2O. After the solvent was decanted off, the polymer was dried under vacuum for 48 h, thus yielding 1.24 g of ABP as a white powder in an 83.0% yield.

2.5 Preparation of PSf-*g*-PMMA and PSf-*g*-PAA

PSf-*g*-PMMA and PSf-*g*-PtBA were prepared through similar procedures as that followed for PSf-*g*-(PMMA-*r*-PtBA) and from the same precursory polymers by setting the [-N_3]/[-C≡CH] feed ratio at a fixed value of 10/1. PSf-*g*-PMMA and PSf-*g*-PtBA were obtained in yields of 85.3%, and 89.7% respectively. After the PtBA chains had been converted to PAA chains via hydrolysis, PSf-*g*-PAA was obtained in an 82.6% yield.

2.6 Preparation of the membranes

Membranes were fabricated via a phase inversion method.[8, 12, 20] In general, casting solutions were prepared by dissolving PSf and ABP in NMP. The overall polymer concentrations were kept constant at 15 wt%, while the ABP weight contents

in the overall polymer/copolymer mixture were varied, i.e. 0, 2, 4, 8, and 16 wt%. The resulting solutions were left to stand for at least 24 h to allow the complete release of bubbles. Secondly, the transparent casting solutions were cast onto glass plates using a 100 μm gate-size stainless steel knife. The casting solution films that covered the glass plates were exposed to the air for 10 s and then immediately immersed into a mixed coagulation bath consisting of DMF/H_2O at various compositions, which was thermo-stated at a certain temperature. The obtained membranes were washed thoroughly with deionized water, and then dried in a dryer at ambient temperature for 24 h before they were annealed in an oven at 60 ^oC for 24 h. The thickness of each membrane was measured with a thickness gage to be 40-50 μm.

2.7 Characterizations

Nuclear Magnetic Resonance (NMR) Spectroscopy. ^1H NMR spectra were recorded using a Bruker DRX-400 spectrometer that was equipped with a Varian probe. The samples were recorded in deuterated chloroform ($CDCl_3$) or dimethyl sulfoxide (DMSO-d_6) at 25 °C. The concentration of each sample was ~10 mg/mL.

Size Exclusion Chromatography (SEC). The number-average molecular weight (M_n) and polydispersity index (M_w/M_n) of each polymer were determined at 35 ^oC using a Waters 1515 size exclusion chromatograph (SEC) equipped with a Waters 2414 refractive index (RI) detector. A DMF solution containing tetrabutylammonium bromide (0.05 mg/L) or alternatively THF was used as the eluent. The SEC system was equipped with styragel HR3 and HR4 columns, which

were calibrated with narrowly dispersed PS standards.

Fourier Transform Infrared (FT-IR) Spectroscopy. The FT-IR spectrum of P(Sf-CH_2N_3) was recording using a FT-IR (Perkin-Elmer Spectrum One) spectrophotometer. The samples were dissolved into acetone and then added dropwise onto a potassium bromide (KBr) pellet and dried under an infrared lamp before characterization.

Scanning electron microscopy (SEM). Surface and cross-sectional images of the membranes were characterized using a scanning electron microscope (SEM, Hitachi, S-4800) that was operated at an accelerating voltage of 2.0 kV. To obtain the cross-sectional images, samples were fractured after they had been soaked in liquid nitrogen for ~5 min. The samples were coated with a thin layer of gold using a Hummer I sputter coater before observation.

Atomic Force Microscopy (AFM). The dried membranes were fixed onto a sample stage and then observed using a MultiMode 8 SPM AFM system (Bruker) that was operated in the Tapping mode.

X-ray Photoelectron Spectroscopy (XPS). XPS measurements were performed using a Surface Science Instruments X-ray Photoelectron Spectroscopy/ESCA (ESCALAB 250, produced by Thermo Fisher Scientific) and operated at a base pressure of ~2×10^{-9} mbar. The samples were irradiated with monochromatic Al Ka X-rays (1486.6 eV) using an elliptical X-ray spot size with a diameter of 500 μm and a power of 15 kV and 150 W. The data were recorded by

setting the take-off angle of the X-rays at 45°. CAE was used as the scanning mode, and the lens model was Large Area XL. Survey spectra were recorded with passing energy of 150 eV, from which the surface chemical compositions were determined.

Determination of the carboxyl group content (CGC). The carboxyl group content (CGC) arising from the PAA chains located on the membrane surface and on the membrane pore walls was evaluated with a well established method based on complexation between the fluorescent dye THA and the PAA carboxyl groups.[54, 55] After equilibration and subsequent washing, the THA is released under acidic conditions and can thus be measured in solution. For this purpose, the membrane sample was initially immersed into a THA solution in ethanol at 10 mmol/L, and shaken for 24 h at room temperature. Subsequently the sample was removed from the solution, and thoroughly rinsed three times with 20 mL of ethanol for 30 s before it was immersed into 10 mL of a 0.01M HCl solution consisting of ethanol/water at 1/1 (v/v). After this mixture had been shaken for 2 h, the concentration of THA released into the solution was measured at λ = 594 nm via UV/vis spectroscopy (UV-1750, SHIMADZU). A plot of THA standards was recorded and used in order to determine the THA concentration in this sample. The CGC was reported with respect to the specific surface area of the membrane sample, and expressed as the content of carboxyl groups per square centimeter of the membrane surface or membrane pore walls in units of pmol/cm^2. The specific surface area of the corresponding membrane sample was analyzed via low temperature (77.38 K) nitrogen adsorption and calculated according to the isotherm of the Brunauer, Emmett

and Teller (BET) model using an Autosorb-iQ-2 (Quantachrome, USA) system.

Mechanical Strength Measurements. All membrane specimens had dimensions of 10 cm × 1 cm. These samples were dried at 60 ^{o}C for 24 h under vacuum and stored in desiccators at room temperature for 48 h prior to tensile mechanical strength measurements. The mechanical properties of all of the specimens, including their tensile strength and the elongation at their breaking point were conducted on a CMT 7503 Universal Testing Machine (Shenzhen SANS Testing Machine Co., Ltd., Shenzhen, China) at a tensile rate of 20 mm/min. Five trials were performed for each sample and the average value was reported.

Water Contact Angle (WCA) Measurements. The water contact angles (WCAs) between water and the membranes were directly measured using a contact angle measuring instrument (Powereach Digital Technology Equipment Co., Ltd., Shanghai, China) in order to evaluate the hydrophilicity of the membranes. Deionized water was used as the probe liquid in all of the measurements. A 5 μL droplet of water was suspended from the tip of a syringe and then moved downward so that it came into contact with the surface of each sample. Upon contact, the sessile droplet became attached onto the surface while pictures were captured by a video system to derive the contact angle information until stable contact angles were reached. The presented WCA of a sample represented the average value obtained from at least five different locations.

Hydraulic permeability tests of the membranes. Round, flat pieces of

membranes, which each had a diameter of 25 mm, were used to test the flux of pure water with Millipore 8010 stirred ultrafiltration cell (Millipore Corporation, Bedford, MA 01739 U.S.A) that had an internal diameter of 25 mm and an effective membrane area of 4.1 cm^2. Before the filtration experiments, the original or modified membranes were pressurized with deionized water for 30 min at 760 mmHg. All of the ultrafiltration experiments were performed at a pressure of 760 mmHg at 25 ^oC. The water flux (*J*) was calculated according to the equation: $J = V/(A \bullet t)$, where *V* corresponds to the volume of the permeate (mL), *A* is the effective membrane area (m^2), and *t* is the sampling time (h).

Evaluation of the stability of the hydrophilicity of membrane. Membranes were soaked in water or in a water/DMF mixture at 80/20 (v/v) at 80 ^oC in a sealed flask, and two samples were collected at predesigned time intervals. The membranes were sequentially rinsed with water and then methanol before they were dried under vacuum at room temperature for 24 h. WCA measurements were performed on the membrane according to the method described above.

3. Results and Discussion

The targeted PSf-*g*-(PMMA-*r*-PAA) was synthesized using the reactions depicted in Scheme 2. First, commercial PSf with M_n = 39,000 g/mol was chloromethylated to yield P(Sf-CH_2Cl). The chlorine atoms were then substituted with azide to yield P(Sf-CH_2N_3). Meanwhile, PMMA and poly(*tert*-butyl acrylate) (PtBA) chains

bearing one terminal alkyne group per chain (PMMA-C≡CH and PtBA-C≡CH) were prepared.[56, 57] The attachment of these chains to P(Sf-CH_2N_3) via click chemistry yielded PSf-*g*-(PMMA-*r*-PtBA).[58]

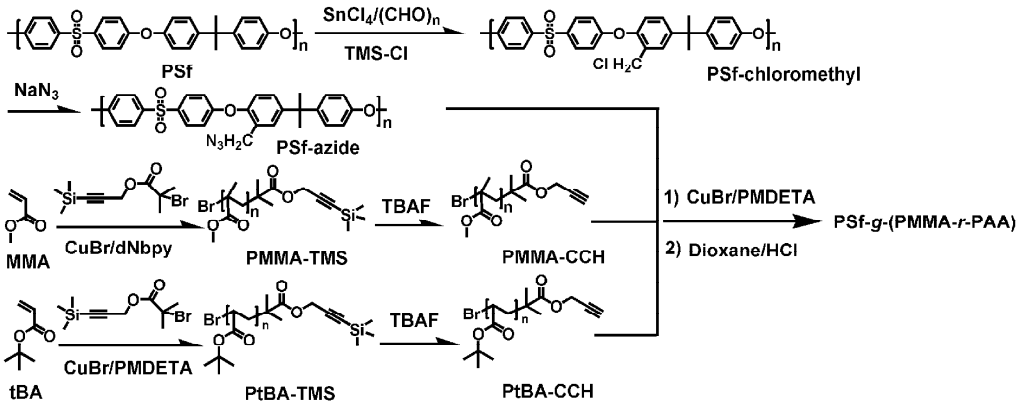

Scheme 2. Synthetic routes towards the amphiphilic graft copolymer.

P(Sf-CH_2N_3). P(Sf-CH_2Cl) and P(Sf-CH_2N_3) were prepared according to a modified literature procedure as described in the experimental section.[58] Figure 1a compares the ^{1}H NMR spectra with peak assignments for PSf, P(Sf-CH_2Cl) and P(Sf-CH_2N_3).[58] The appearance of signal labeled as (5) at 4.52 ppm corresponding to protons of the chloromethyl (-C*H*$_2$Cl) group demonstrated the successful preparation of P(Sf-CH_2Cl). This peak, however, shifted to 4.26 ppm in the spectrum of P(Sf-CH_2N_3), in agreement with the substitution of -Cl by -N_3 and thus supporting P(Sf-CH_2N_3) synthesis. Moreover, the complete disappearance of the signal at 4.52 ppm demonstrated the quantitative nature of this SN2 reaction. The successful preparation of P(Sf-CH_2N_3) was also demonstrated via FT-IR analysis by the appearance of a characteristic absorption peak at 2104 cm^{-1} corresponding to the azide group (Figure 1b).

The degree of substitution (DS), defined as the fraction of Sf units that had been substituted, could also be obtained from the ^{1}H NMR spectra. For P(Sf-CH_2Cl), the DS was calculated as 0.6 by comparing the integrals of peak (5) at 4.52 ppm to the peak at 7.85 ppm corresponding to the four *meta* protons on the phenyl ring closest to the sulfonyl group. Meanwhile, the DS of P(Sf-CH_2N_3) was found to be 0.6 as determined by comparison of the integral of the signal (6) at 4.26 ppm to that of the peak at 7.85 ppm corresponded to the four *meta* protons on the phenyl ring closest to the sulfonyl group. The DS corresponding to the chloromethylation of PSf and that representing the azidomethylation of PSf had a similar value of 0.6, thus indicating that the -CH_2Cl groups of P(Sf-CH_2Cl) were quantitatively converted to -CH_2N_3 groups.

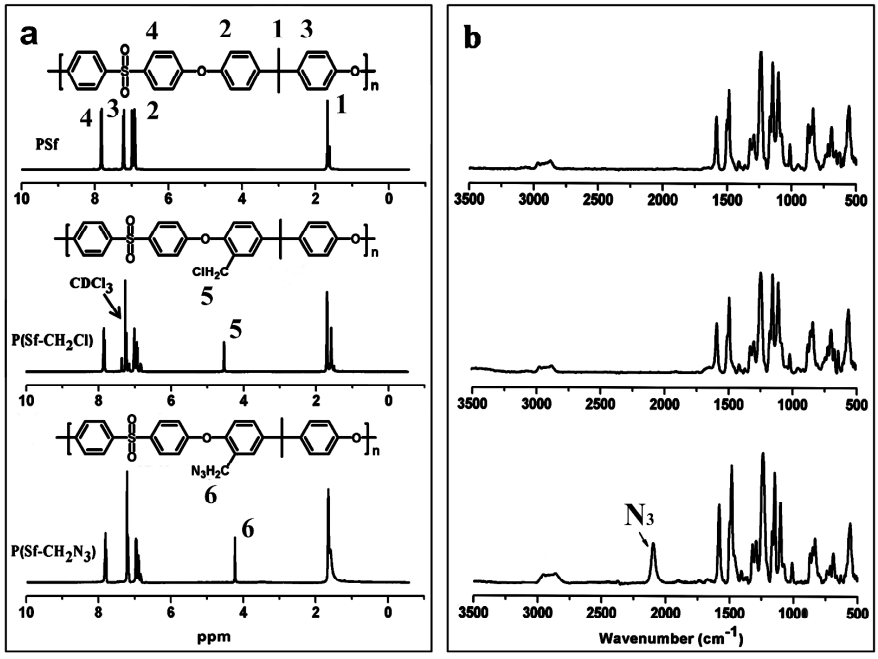

Figure 1. ^{1}H NMR (a) and FT-IR (b) spectra of PSf (top), P(Sf-CH_2Cl) (middle) and P(Sf-CH_2N_3) (bottom spectra).

PMMA-C≡CH and PtBA-C≡CH. PMMA-C≡CH and PtBA-C≡CH were prepared via two steps, which included the atom transfer radical polymerization (ATRP) of the corresponding monomers and the deprotection of the trimethylsilyl groups that had been introduced by the initiator (Scheme 2).[52] Both polymerizations were performed in a similar manner using 3-(trimethylsilyl)-propargyl 2-bromoisobutyrate as the initiator and by using CuBr/dNbpy as well as CuBr/PMDETA as the catalyst systems to yield PMMA-C≡CSi$(CH_3)_3$ and PtBA-C≡CSi$(CH_3)_3$. The targeted PMMA-C≡CH and PtBA-C≡CH polymers were obtained after the removal of the trimethylsilyl group from their corresponding precursors by stirring the polymers with tetrabutylammonium fluoride in CH_2Cl_2.[52]

The resulting precursory polymers were characterized by ^{1}H NMR using $CDCl_3$ as the solvent and by SEC using THF as the eluent. Figure 2 compares ^{1}H NMR spectra of PMMA-C≡CSi$(CH_3)_3$, PMMA-C≡CH, PtBA-C≡CSi$(CH_3)_3$, and PtBA-C≡CH together with their peak assignments. The complete removal of the trimethylsilyl group from PMMA-C≡CSi$(CH_3)_3$ or PtBA-C≡CSi$(CH_3)_3$ was confirmed by the disappearance of the proton signals (6) at 0.16-0.17 ppm. In addition, the agreements between the observed and expected peaks demonstrated our success synthesis of the targeted polymers.

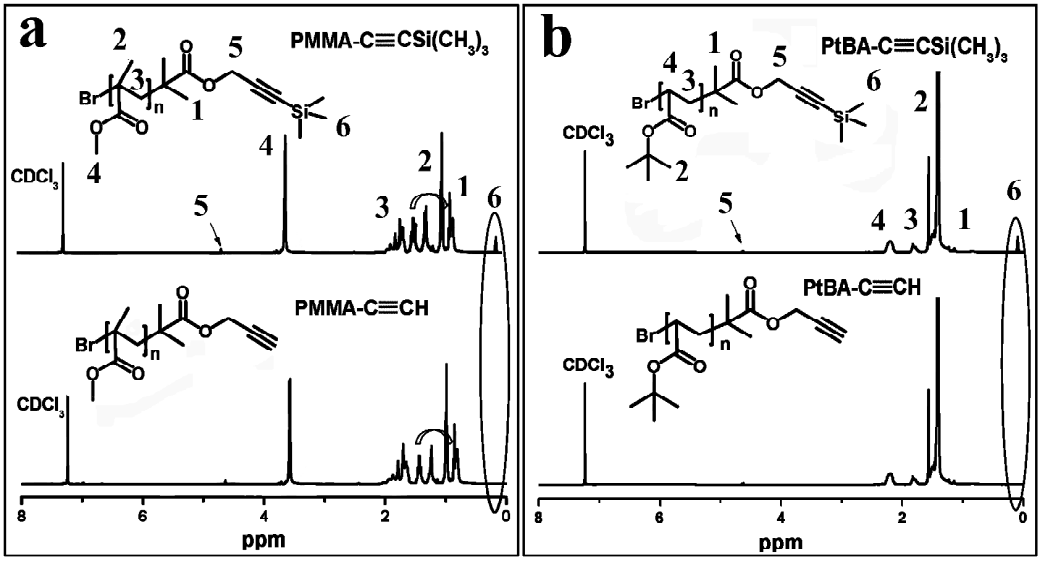

Figure 2. ^{1}H NMR spectra of the polymers PMMA-C≡CSi$(CH_3)_3$ and PMMA-C≡CH (a), and PtBA-C≡CSi$(CH_3)_3$ and PtBA-C≡CH (b).

The degree of polymerization (*DP*) of PMMA-C≡CH and PtBA-C≡CH were determined ^{1}H NMR by comparing the integrations of the -OCH_3 (4) protons of PMMA-C≡CH at 3.67 ppm and that of the –$OC(CH_3)_3$ (2) protons of PtBA-C≡CH at 1.43 ppm to that of the -CH_2-C≡C- (5) protons observed for both polymers at 4.63 ppm. From these comparisons, the *DP* of PMMA-C≡CH and PtBA-C≡CH were found to be 51 and 54, respectively. The *DP* values were also evaluated from the products by comparing the monomer-to-initiator molar ratios and the gravimetric yields of the polymers. This protocol yielded the *DP* values of 49 and 52, respectively, for the two polymers. The numbers determined from the different methods were in close agreement with each other. Our SEC analyses yielded polydispersity indices of < 1.22 for the two polymers (Table 1).

Table 1. Preparation conditions and structural characteristics of the polymers.

Sample	$[M]_o/[I]_o$	Yield (%)	NMR *DP*	NMR M_n (kg/mol)	SEC[a] M_w/M_n

P(Sf-CH_2Cl)	---	---	---	---	1.64
P(Sf-CH_2N_3)	---	---	---	---	1.65
PMMA-CCSi$(CH_3)_3$	100/1	49.4	51	5.4	1.23
PMMA-C≡CH	---	87.5	51	5.3	1.22
PtBA-CCSi$(CH_3)_3$	100/1	52.2	54	7.2	1.20
PtBA-C≡CH	---	89.1	54	7.1	1.20

	Molar ratio[b] **from NMR**	f_{PMMA}[c] (wt%)	f_{PAA}[c] (wt%)	**NMR M_n (kg/mol)**	M_w/M_n[d]
PSf-*g*-(PMMA-*r*-PAA)	1/3.0/3.1	31	23	101.6	1.22
PSf-*g*-PAA	1/3.2	---	34	63.4	1.23
PSf-*g*-PMMA	1/3.0	40	---	43.1	1.26

[a]THF was used as the eluent. [b] [Sf]:[MMA]:[tBA]. [c]The mass percentage of the side chains in the total copolymers. [d]DMF was used as the eluent.

PSf-*g*-(PMMA-*r*-PAA). PSf-*g*-(PMMA-*r*-PtBA) was prepared by reacting P(Sf-CH_2N_3), PMMA-C≡CH, and PtBA-C≡CH at a [-N_3]:[PMMA-C≡CH]:[PtBA-C≡CH] molar ratio of 10/1/1 using CuBr/PMDETA as the catalyst system.[50, 52] The crude product was passed through a neutral alumina column to remove metal salts, concentrated, and then added into water to precipitate the polymer. Heating the resultant polymer at 100 °C in a dioxane solution containing HCl selectively hydrolyzed PtBA to yield PSf-*g*-(PMMA-*r*-PAA).

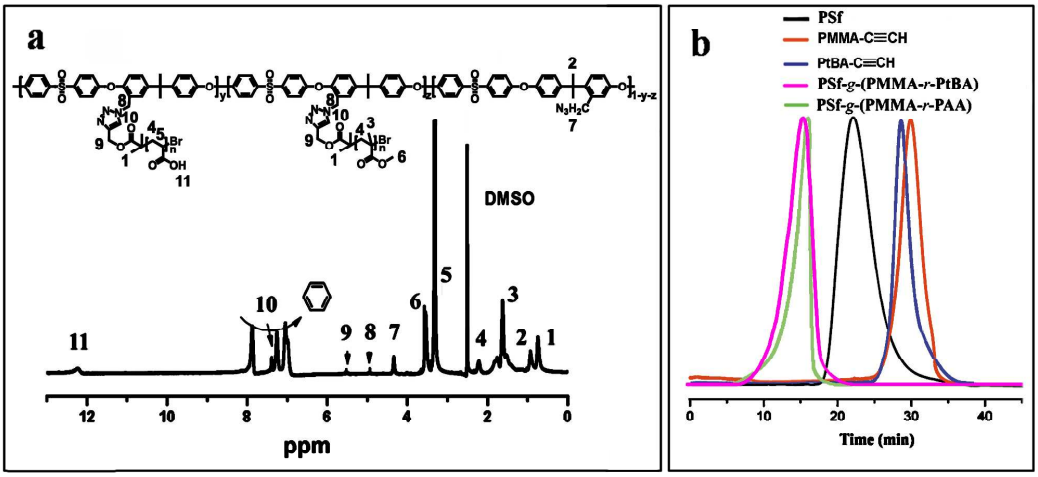

Figure 3. ^{1}H NMR spectrum of PSf-*g*-(PMMA-*r*-PAA) recorded in DMSO-d_6 (a) and SEC traces of P(Sf-CH_2N_3), PtBA-C≡CH, PMMA-C≡CH, PSf-*g*-(PMMA-*r*-PtBA), and PSf-*g*-(PMMA-*r*-PAA) recorded using DMF as the eluent (b).

Figure 3a shows the ^{1}H NMR spectrum of PSf-*g*-(PMMA-*r*-PAA) along with peak assignments. The characteristic signals corresponding to PAA and PMMA were clearly observed. Furthermore, the signal at 4.93 ppm corresponding to the methylene protons next to the 1,2,3-triazole groups was observed, and a new peak at 7.35 ppm can be attributed to the methine proton of the 1,2,3-triazole groups. This indicated that the click reaction was successful. The ratio of [Sf]/[MMA]/[AA] in the PSf-*g*-(PMMA-*r*-PAA) was 1/3.0/3.1. This ratio was determined by comparing the integration of the signal at 7.85 ppm corresponding to the four *meta* protons on the phenyl ring closest to the sulfonyl group, with that of the -OCH_3 signal for PMMA at 3.67 ppm and with the integration of the remaining -CH_2N_3 protons in the PSf backbone at 5.26 ppm. This value was comparable to the feed ratio of 1/3.1/3.1 for [Sf]/[MMA]/[AA], suggesting that the precursors were nearly completely grafted onto the backbone.

The SEC traces measured using DMF as the eluent were compared in Figure 3b for P(Sf-CH_2N_3), PMMA-C≡CH, PtBA-C≡CH, and the crude reaction mixture after the click reaction without purification. DMF was used in this case because the graft copolymer had more soluble in DMF than in THF. As expected, PSf-*g*-(PMMA-*r*-PtBA) had a much shorter retention time than those of its precursors. More interestingly, no SEC peaks corresponding to the precursors were observed for

the reaction mixture, suggesting that the grafting reactions were quantitative due to low molar ratios used for the alkyne and azide groups. In addition, the apparent SEC molecular weight of PSf-*g*-(PMMA-*r*-PAA) decreased only slightly relative to that of PSf-*g*-(PMMA-*r*-PtBA), in agreement with the cleavage of the *tert*-butyl groups.

Since the polymer side chains with known *DP*s were completely grafted onto the backbone, the average *DP* of PSf could be calculated as ~90, by comparison the integration of the PMMA signal appearing at 3.67 ppm to that of the PSf signal appearing at 7.85 ppm. Therefore, the [-N_3]:[PMMA-C≡CH]:[PtBA-C≡CH] molar feed ratios of 10/1/1 suggested that each PSf chain contained 5.3 PMMA and 5.2 PAA chains, respectively. The mass fractions of PAA and PMMA in this graft copolymer were 23 wt%, and 31 wt%, respectively.

For comparison, two other graft copolymer samples, PSf-*g*-PMMA and PSf-*g*-PAA, were prepared through similar procedures as that for PSf-*g*-(PMMA-*r*-PAA) by fixing the [-N_3]:[-C≡CH] molar feed ratio at 10/1. The results demonstrate that PMMA or PAA chains were also quantitatively attached onto the PSf backbone. The mass fraction of PAA in PSf-*g*-PAA and PMMA in PSf-*g*-PMMA were 34 wt% and 40 wt%, respectively.

Effect of Varying the Coagulation Bath Composition on the Membrane Formation. Membranes were prepared through the following four steps: 1) dissolving PSf in the presence or absence of PSf-*g*-(PMMA-*r*-PAA) in *N*-methyl pyrolidone (NMP); 2) casting these solutions as films onto glass plates; 3) soaking these films for 30 min in a coagulation bath that contained a mixture of DMF and

water to induce membrane formation by phase inversion; and 4) annealing these membranes at room temperature for 24 h and then at 60 ^{o}C for 24 h after they had been thoroughly rinsed with deionized water. Thus, factors such as the polymer concentration in the casting solution, coagulation bath parameters including its temperature, pH value, and DMF volume fraction (f_{DMF}), as well as the membrane annealing times and temperature should influence the final membrane structure.

To examine the effect of varying the coagulation bath parameters, we initially fixed the total polymer concentration in NMP to 15 wt% and the mass fraction of PSf-*g*-(PMMA-*r*-PAA) among the used polymers to 2.0 wt%. We also used the same membrane annealing conditions as mentioned above. Under these conditions, we prepared three families of membranes denoted as M2-f_{DMF}, M2-T, and M2-pH, where M2 indicates that the PSf-*g*-(PMMA-*r*-PAA) mass fraction among the used polymers was 2.0 wt%. Meanwhile, f_{DMF}, T, and pH suggest that only the DMF volume fraction, the bath temperature, and the bath pH was varied among samples of a given series. Table 2 specifies other parameters used to prepare the three series of samples.

Table 2. Coagulation bath parameters used for preparing the three families of membranes.

Entry	f_{DMF}	Temperature (^{o}C)	pH value
M2-f_{DMF}	0-100	20	7
M2-T	80%	20-60	7
M2-pH	80%	20	2-12

We characterized the three series of membranes prepared using the conditions

specified above by measuring the carboxyl group contents and WCAs of the membrane surfaces and the results of these measurements are summarized in Figure 4a–4c. To measure a WCA, a water droplet was dispersed onto a membrane before a picture was taken of the droplet and the droplet behavior was analyzed. To obtain the carboxyl group content (CGC) in terms of the moles of carboxyl groups per cm^2 of membrane specific surface area, a literature method was used.[55] In this procedure, a prepared membrane was equilibrated with thionin acetate. Surface carboxyl groups have been shown to bind at a 1:1 molar ratio with thionin cations solubilized in ethanol when thionin acetate was used in excess. The thionin-adsorbed membrane was then rinsed with ethanol and thionin was quantitatively released when the membrane was finally rinsed with an acidic ethanol/water solution. During this process, the thionin binding and release was clearly indicated by a change in the membrane's color from white to blue (in the case of binding) and back to white (in the case of release, see Figure S1 in the Supporting Information).

The WCA data in Figures 4a – 4c evidently mirrored (with respect to a horizontal plane) the variation trends of the CGC data. When the WCAs increased, the CGC values decreased, which was consistent with the intuition that carboxyl groups helped hydrophilize the surfaces and thus decreased their WCAs.

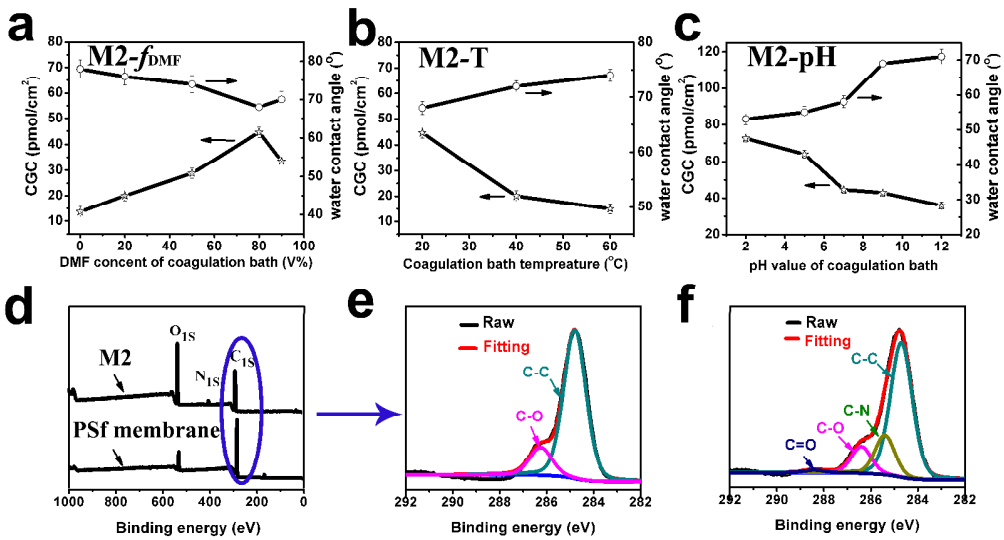

Figure 4. Variation of the CGC and WCA as a function of f_{DMF} (a), temperature (b), and pH (c) of the coagulation bath. Also shown are the survey XPS spectra (d) and high-resolution C_{1s} XPS spectra (e and f) of a PSf membrane and a M2 membrane prepared at pH = 2.0, f_{DMF} = 80%, and T = 20 °C.

As f_{DMF} increased, the CGC increased initially until f_{DMF} reached 80%. We further noted by naked eye observations that the time required for the film to turn white from clear increased as f_{DMF} increased. Thus, increasing f_{DMF} improved the compatibility between the coagulation fluid and the polymer PSf and lengthened the time required for the polymer to vitrify. A reasonable inference here was that PSf-*g*-(PMMA-*r*-PAA) had more time to segregate and thus allow the PAA domains to enrich the pore and membrane surfaces as f_{DMF} increased.

However, the CGC decreased as f_{DMF} was increased from 80% to 90%. This CGC decrease might be caused by the solubility of PSf-*g*-(PMMA-*r*-PAA) in DMF/water at f_{DMF} = 90% and the detachment of many PSf-*g*-(PMMA-*r*-PAA) chains from the membrane surfaces. In a control experiment, we dissolved PSf-*g*-(PMMA-*r*-PAA) in DMF at ~2 wt% and then added water dropwise into this

solution. At f_{DMF} = 90%, no polymer precipitation was observed. On the other hand, most of the polymer had precipitated when f_{DMF} was decreased to 80%. Therefore, f_{DMF} = 80% was used herein unless otherwise mentioned.

We note that the CGC decreased with temperature T for the M2-T series. Indeed, the diffusion rate of PSf-*g*-(PMMA-*r*-PAA) should increase with T to promote graft copolymer surface segregation. A higher T also facilitated solvent diffusion and increased the rate of polymer vitrification. Our speculation was that the overall effect of increases in T was to decrease the CGC. Thus, our membranes were prepared in coagulation baths set at 20 ^{o}C unless mentioned otherwise.

The data shown in Figure 4c reveals that the CGC decreased as the pH of the coagulation bath increased. We did not examine the cause for this trend. Our speculation was that the solubility of PSf-*g*-(PMMA-*r*-PAA) in DMF/water at f_{DMF} = 80% increased with increases in the pH due to the deprotonation of the AA carboxyl groups. This increased solubility could have extracted more PSf-*g*-(PMMA-*r*-PAA) chains into the coagulation bath. Therefore, we used pH = 2.0 in our subsequent preparations.

In summary, our above experiments established that the optimal coagulation bath parameters were pH = 2.0, T = 20 ^{o}C, and f_{DMF} = 80%. Using these parameters, we have prepared samples that are denoted as M2. On these membranes, the CGC and WCAs were 72.6 pmol/cm^2 and 53°, respectively.

We further confirmed the surface enrichment of the carboxyl groups of M2 membranes by XPS. While Figure 4d shows the survey XPS spectra of a M2

membrane and a PSf membrane, the high-resolution C_{1s} spectra of the M2 and PSf membranes are compared in Figures 4e and 4f, respectively. Our quantitative analyses yielded the atomic and functional molar fractions in the probed surface regions and these results are summarized in Table 3.

Table 3. Atomic and functional abundances calculated from polymer compositions and those evaluated from the survey XPS spectra shown in Figure 4d and high resolution C_{1s} spectra shown in Figures 4e-4f.

Samples*	O[#] (%)	S[#] (%)	N[#] (%)	C[#] (%)	C[#] (%)			
					C-C	C-O	C=O	C-N
PSf[a]	12.50	3.12	---	84.38	76.71	7.67	---	---
M2[a]	12.76	3.08	0.04	84.12	76.23	7.75	0.12	0.02
PSf[b]	12.98	3.02	---	84.00	75.87	8.13	---	---
M2[b]	35.28	0.24	3.47	61.01	45.46	9.24	5.79	0.52

[a] Theoretical values calculated based on the bulk composition of PSf membranes or M2 membrane; [b] Mean values evaluated from three separate experiments with a standard deviation of ± 0.05%.

The appearance of a N_{1s} peak at 400.2 eV corresponding to the triazo nitrogen atoms and the high intensity of O_{1s} peak in the survey spectrum measured for the M2 membranes demonstrated the successful enrichment of the surfaces by PSf-*g*-(PMMA-*r*-PAA). The surface enrichment by carboxyl groups was further supported by the carbonyl functional group content of 5.79%, as revealed by the high-resolution deconvolution analysis of the C_{1s} peak. This observed carbonyl functional group content value was much higher than the calculated value of 0.12% that would be expected for a bulk PSf sample containing 2.0 wt% of

PSf-*g*-(PMMA-*r*-PAA) based on the chemical structure and composition (Table 3).

Effect of Varying the PSf-*g*-(PMMA-*r*-PAA) Content on the Membrane Formation. Using the optimized parameters for the coagulation bath we prepared membranes containing different PSf-*g*-(PMMA-*r*-PAA) mass fractions, w_g, in the used PSf and graft copolymer mixtures. These samples were denoted as M0, M2, M6, M8, and M16, indicating that w_g assumed the values of 0, 1.0, 2.0, 4.0, 6.0, 8.0, and 16.0 wt%, respectively. Reported in Figures 5a-5b are the variations in the measured CGCs and WCAs as a function of w_g. The CGC increased initially with w_g and then leveled off above w_g = 8.0 wt%, suggesting that a maximum enrichment of PSf-*g*-(PMMA-*r*-PAA) on the membrane surface and membrane pore walls could be reached at w_g = 8.0 wt% using the optimal coagulation bath parameters.

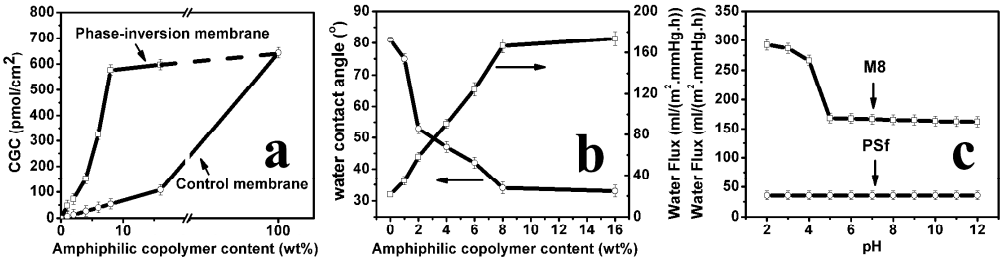

Figure 5. Variations in the surface CGC (a), the WCA (b, left axis), and the water flux of membranes (b, right axis) as a function of the graft mass fraction in the polymer mixture used to prepare membrane, or w_g. Also shown is the variation in the water flux of a M0 (PSf) membrane and a M8 membrane as a function of the pH (c).

Membranes of the M*x* series were prepared by the phase inversion method, which promoted the surface segregation of PSf-*g*-(PMMA-*r*-PAA). We prepared control membranes from this series of polymer mixtures using another method. In this

approach, the cast solution films were partially dried initially in a desiccator flushed with dry N_2 and subsequently dried fully under vacuum at 60 ^oC for 72 h. Since the polymer solution never came into contact with moisture or water during film formation, we suspected that surface enrichment by PSf-*g*-(PMMA-*r*-PAA) should be suppressed for this series of membranes. The CGCs were also measured for this series of control membranes and these results are plotted in Figure 5a. The CGC on the membrane prepared via phase inversion at w_g = 8 wt% was 576.6 pmol/cm^2, which was more than ten times higher than the value of 54.3 pmol/cm^2 measured on the corresponding control membrane. In addition, the membrane M8 prepared via phase inversion had a CGC comparable to that of 643.4 pmol/cm^2 measured on a control membrane made from pure PSf-*g*-(PMMA-*r*-PAA). Thus, the surface segregation effect of PSf-*g*-(PMMA-*r*-PAA) was fairly evident for membranes prepared through the phase inversion method.

Water fluxes for this set of membranes were also measured. As seen in Figure 5b, the water flux increased with increases in w_g, but leveled off above w_g = 8.0 wt%. While water flux of a M2 membrane was 57.9 mL/(m^2·mmHg·h), it increased to 166.3 mL/(m^2·mmHg·h) for a M8 membrane.

More interestingly, the M8 membrane exhibited pH-dependent water flow. As the pH of the aqueous phase was increased from 2.0 to 5.0, the water flux decreased from 292 to 168 mL/(m^2·mmHg·h). This was in stark contrast to the behavior of the M0 membrane, which had a constant water flux ~21 mL/(m^2·mmHg·h) between pH 2.0 and 12.0. The pH-responsiveness must be due to the contraction of the PAA

chains at low pH values and their extension at high pH values. The extension of the PAA chains from the walls of the pores caused the pore dimensions to shrink and thus reduced the water flow.[21, 59] Such pH-responsiveness of the membranes provided direct evidence that the enrichment of PAA occurred not only on the membrane surface but also membrane on the pore walls.

Membrane Morphologies. Morphologies of M0, M2, M8, and M16 membranes were examined via SEM and AFM techniques. While the surface morphologies of these membranes are compared in Figures 6a-6d, their cross-sectional images are shown in Figures 6e-6h.

The surface SEM images show that the PSf membrane (or M0) exhibited a relatively smooth surface, as is typically observed for a PSf membrane prepared through the immersion precipitation process.[20] No obvious pores could be discerned at a 40,000X magnification. In contrast, pores became clearly visible and both their average diameter and quantity increased when w_g was increased from 2% to 16%.

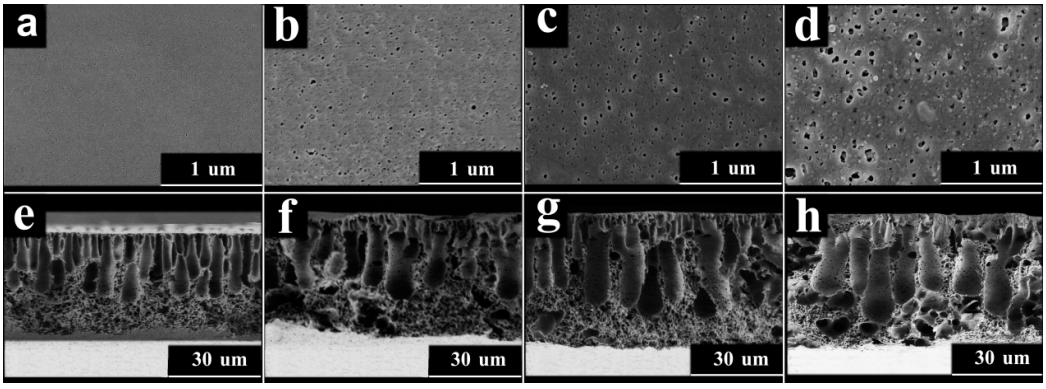

Figure 6. SEM images of surfaces (a-d) and cross-sections (e-h) of M0, M2, M8, and M16 membranes. The membranes shown above proceed from M0, to M2, to M8, and to M16 membranes as one views the Figure from left to right.

The cross-sectional images show that all of the membranes exhibited the characteristic morphology of asymmetric membranes and were covered by a dense top skin-like layer and incorporated finger-like macrovoids underneath this layer. As w_g increased, the finger-like structures became wider. The widening of these fingers has been traditionally associated with a slowing down in the vitrification of the polymer phase during membrane formation and suggested that the PSf-*g*-(PMMA-r-PAA) additive provided stability to the phase-separating PSf polymer. This slower PSf vitrification was probably also responsible for the increased pore sizes and numbers observed on the membrane surface (Figures 6a-6d) as w_g increased. Thus, the addition of PSf-*g*-(PMMA-r-PAA) not only enhanced the hydrophilicity of the membrane and its pore surfaces but also changed the pore structures. Additionally, the change in the pore structures is mainly responsible for the dramatic increase observed in the water flux of the PSf-*g*-(PMMA-*r*-PAA)-containing membranes relative to that of the M0 membranes.

AFM images were recorded in the tapping mode to probe the structure of the membrane surface. The AFM topography images shown in Figure 7a clearly demonstrate that the surface roughness increased as w_g increased. A more quantitative analysis revealed that the average roughness increased from 5.3 nm to 8.9 nm, to 9.8 nm, and to 12.8 nm as one proceeded from M0, to M2, to M8, and to M16, respectively. In addition, interconnected cavities among the granules or nodules (hills and valley), and agglomerated-nodules were clearly visible. Such typical "spinodal" structure is frequently observed among membranes prepared via the phase

inversion method.[60-62] Figure 7b compares AFM phase images for the corresponding membranes. Interestingly, while no obviously white domains were observed in the AFM phase image for the PSf (or M0) membrane, white nano-domains were visible among the membranes containing PSf-*g*-(PMMA-r-PAA). Moreover, the average size and the density of the white domains increased with increases in w_g. These white domains must have been associated with the presence of PAA chains in the PSf-*g*-(PMMA-*r*-PAA) rather than PMMA or PSf. Further evidence for this assignment was provided by the fact that no white domains were observed in the AFM phase image of the PSf membrane containing 8 wt% of PSf-*g*-PMMA prepared under identical conditions to that for M8. Therefore, these PAA domains could be detected in the phase images and thus AFM provided further evidence supporting the segregation of PSf-*g*-(PMMA-*r*-PAA) and that the hydrophilic PAA domains aggregated preferentially on the membrane surface.

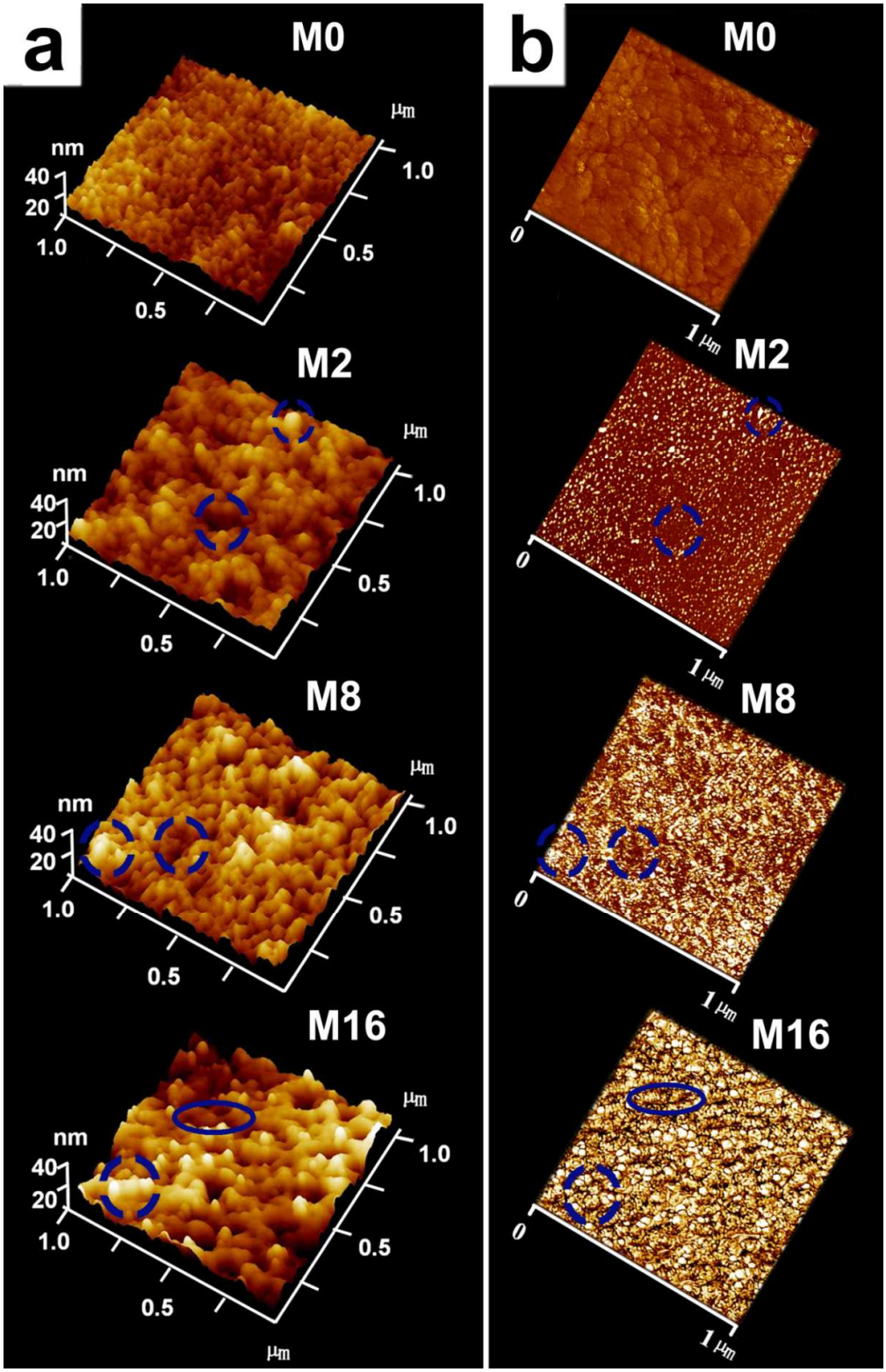

Figure 7. AFM 3-d topography (a) and phase (b) images of the M0, M2, M8, and M16 membranes. The circles inserted in the images are meant to provide a visual guide.

By carefully comparing the AFM phase image with the corresponding AFM 3-d topography image of each specimen, we found that the white nano-domains corresponding to the PAA chains were mainly located as "islands" on the granules, nodules or agglomerated nodules on the surface of the M2 membrane. In contrast, while some of the white nano-domains were located in the cavity channels or the pores, they had conglomerated or even fused together to form a continuous layer that was accompanied by granules or nodules, and agglomerated-nodules as w_g increased to more than 8%. These observations validated our initial assumption that the exposure of the PAA domains on the membrane surface resulted from an enhanced surface enrichment that occurred among the membranes containing more than 8 wt% of PSf-*g*-(PMMA-*r*-PAA).

Probing into Mechanism of Surface Enrichment. In the case of PSf membranes prepared without PSf-*g*-(PMMA-*r*-PAA), it is not surprising that a nodular structure exhibiting with interconnected cavity channels on the membrane surface as formed from liquid-liquid phase separation process via a spinodal decomposition mechanism.[63, 64] However, the amphiphilic nature of the graft copolymer was believed to have a significant impact on the liquid-liquid separation process leading to different membrane morphology. The formation mechanism for the membrane surface through this process is proposed and illustrated in Figure 8. That is, when the homogenous casting solution film containing both PSf and PSf-*g*-(PMMA-*r*-PAA) was immersed into the coagulation bath, the polymer PSf and PSf-*g*-(PMMA-*r*-PAA) also began to separate from each other into PSf-enriched and PSf-poor phases, respectively. The proposal that PSf-*g*-(PMMA-*r*-PAA)

preferentially aggregated at the interface between the PSf-enriched and the PSf-poor phases was based on two considerations. First, due to the amphiphilic nature of PSf-*g*-(PMMA-r-PAA), this copolymer favored the interface between the PSf rich-phase and PSf poor-phase to decrease the interfacial energy between these domains.[33] Second, the chemical potential of PSf-*g*-(PMMA-*r*-PAA) with its hydrophilic PAA chains in water was expected to be less than that of PSf.[33] PSf-*g*-(PMMA-r-PAA) was transported more slowly into the PSf-poor phases than PSf prior to precipitation, causing PSf-*g*-(PMMA-*r*-PAA) to enrich surfaces of the membrane.

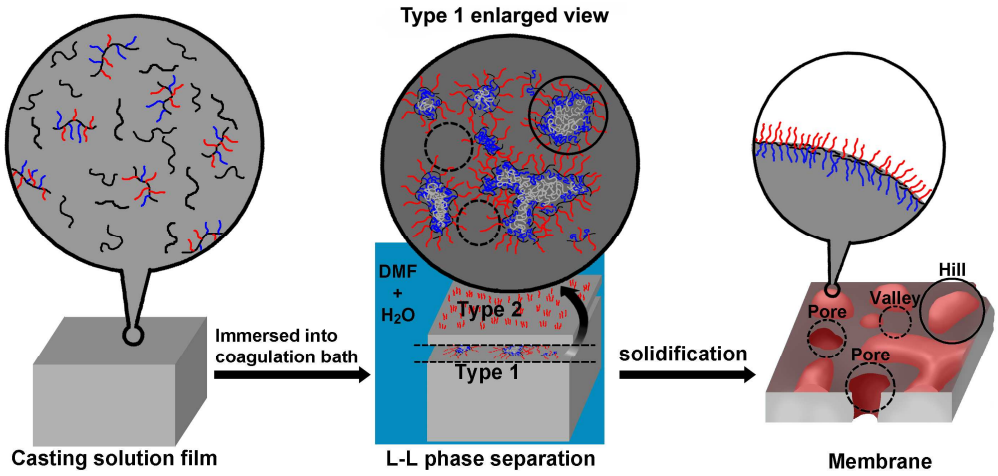

Figure 8. Illustration depicting the formation mechanism for membrane surfaces through a liquid-liquid process. The black, red, and blue chains correspond to PSf, PAA, and PMMA chains, respectively.

It is imagined that the hydrophobic PMMA side-chains of PSf-*g*-(PMMA-r-PAA) were entrapped within the PSf-enriched phase or the PSf-poor phase, whilst the hydrophilic PAA side-chains resided at the interface between the PSf-enriched and the

PSf-poor phases (type 1 in Figure 8), or alternatively at the interface between the coagulation bath and both liquid PSf phases (type 2 in Figure 8). Thus, the granules, nodules or aggregated nodules were eventually developed from droplets of polymer-enriched phases, and the pores corresponding to the interstitial cavities were formed from the polymer-poor phases. This was supported by the fact that PAA tended to position itself on the granules or nodules on the membrane surface as observed in the AFM phase images (Figure 7). Therefore, changes in the copolymer content influenced both the size and density of domains formed by the PSf-lean or PSf-enriched domains, which resulted in changes in the membrane structure. Such structures, bearing PAA chains that enriched the membrane surface and PMMA chains that were isolated within the PSf substrate arose from the entrapment of domains derived from both PSf-enriched and PSf-poor liquid phases, were responsible for the performance of membrane.

Other Properties of M8 Membranes. While the successful hydrophilization of the membrane was evident from the membrane's surface chemistry, topography, and its performance, the long-term stability of the membrane's hydrophilicity was further evaluated for M8 samples that were extracted with different solvents. For comparison, a control membrane prepared from a PSf/copolymer mixture containing 8 wt% of PSf-*g*-PAA under identical conditions as employed for M8 was also evaluated. Membranes were soaked in water or water/DMF at 80/20 (v/v) at 80 ^{o}C in a sealed flask, and two membrane samples were collected at predesigned time intervals. The membranes were sequentially rinsed with water and then methanol

before they were dried under vacuum at room temperature for 24 h. Figure 9a-d shows the dependence of the membrane's WCA and water flux on the soaking time in water or in a water/DMF (80/20, v/v) mixture at 80 °C.

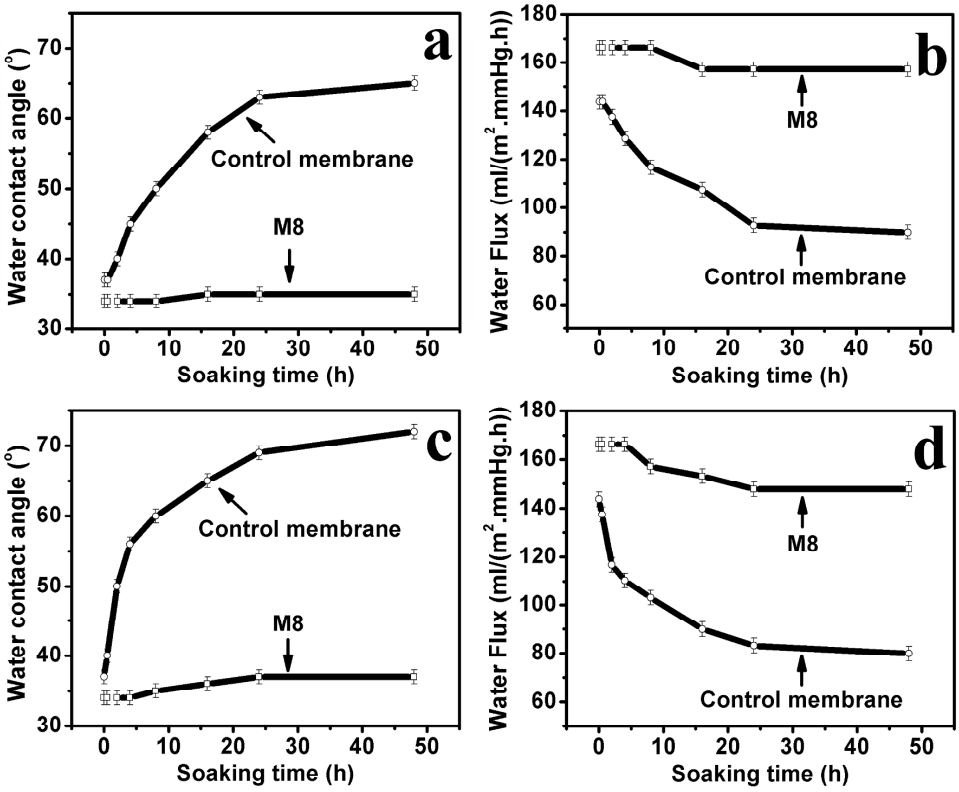

Figure 9. The relationship between the WCAs, water flux of the membranes and the soaking times for samples that were soaked in water (a,b) and in a water/DMF mixture at v/v = 80/20 (c,d).

The control membrane exhibited a WCA of 37° and a water flux of 143.7 mL/(m^2·mmHg·h), which were close to that observed for M8 prior to solvent extraction. The WCA of the control membrane increased dramatically from 37° to 63° within the first 24 h of soaking in water and leveled off at 65° after it had been soaked for 48 h (Figure 9a). In comparison, the WCA increased from 37° to 69° and

to 72^{o} after the membrane had been soaked for similar respective times in water/DMF (Figure 9c). In contrast, the WCAs of M8 did not change significantly. The water flux of the control membrane decreased from 143.7 mL/(m^2·mmHg·h) to 92.8 mL/(m^2·mmHg·h) within the first 24 h of soaking in water and leveled off at 89.9 mL/(m^2·mmHg·h) after it had been soaked for 48 h (Figure 9b). In comparison, the water flux decreased from 143.7 mL/(m^2·mmHg·h) to 83.2 mL/(m^2·mmHg·h) and to 79.9 mL/(m^2·mmHg·h) after the membrane had been soaked for similar respective times in water/DMF (Figure 9d). On the contrary, the water flux of M8 did not change significantly. The variation of the hydrophilicity of the control sample and to a lesser extent M8 undoubtedly resulted from loss of PSf-*g*-PAA or PSf-*g*-(PMMA-r-PAA) from the membrane surface during the solvent extraction treatment. For this purpose, we only tested the CGCs of the M8 and the control membrane before and after they had been subjected to solvent extraction for 48 h. The results show that the CGCs of the control membrane decreased dramatically from 530.1 pmol/cm^2 to 56.3 pmol/cm^2 and to 42.6 pmol/cm^2 after it had been soaked in water and in water/DMF for 48 h, respectively. In contrast, the CGCs of M8 changed only slightly from 564.9 pmol/cm^2 and to ~550.7 pmol/cm^2 after it had been soaked for a similar time period in water and in the water/DMF mixture. This indicated that the hydrophilicity of M8 was significantly more durable than that of the control membrane. This enhanced durability may be attributed to the PMMA chains of PSf-*g*-(PMMA-*r*-PAA) becoming entrapped within the PSf substrate.

To evaluate the effect of the addition of the graft copolymer on the mechanical properties of the membrane, we performed a preliminary evaluation of the tensile strengths and the elongation at the breaking points of M0 and M8. The results show that M8 had a tensile strength of 5.4 ± 0.5 MPa and exhibited an elongation of 12.1 ± 1% at its breaking point, while M0 exhibited corresponding values of 5.7 ± 0.4 MPa and 13.4 ± 1% at its breaking point. These results indicated that the current hydrophilization strategy did not adversely affect the mechanical properties of the membranes.

4. Conclusions

A binary graft copolymer PSf-*g*-(PMMA-*r*-PAA) has been successfully synthesized and characterized. This graft copolymer has been mixed with PSf and used to prepare porous membranes through a phase inversion method. Various experimental parameters including the pH, temperature, and the DMF volume fraction in the coagulation bath as well as the PSf-*g*-(PMMA-*r*-PAA) mass fraction in the PSf/graft copolymer mixture have been systematically studied. In addition, these conditions were optimized to promote the segregation of PSf-*g*-(PMMA-*r*-PAA) and the enrichment of the PAA chains on the surfaces of the membranes and their pore walls. The surface enrichment by the hydrophilic PAA chains has been confirmed by the low WCAs exhibited by these membranes, as well as their high degree of thionin acetate adsorption, and high surface CGCs as determined via XPS and even

from AFM phase images. This optimized preparation strategy yielded PSf/PSf-*g*-(PMMA-*r*-PAA)-based membranes that incorporated only 8 wt% of PSf-*g*-(PMMA-*r*-PAA), and yet exhibited surface CGCs that were comparable to those observed among bulk PSf-*g*-(PMMA-*r*-PAA) films, and with nearly complete surface coverage by PAA. The PSf-*g*-(PMMA-*r*-PAA) additive not only hydrophilized the resultant porous membrane, but also increased the membrane's water flux. The water flux could was also readily tuned by varying the pH. In addition, the surface-anchored PSf-*g*-(PMMA-*r*-PAA) chains were robust and withstood solvent extraction. All of these advantages were achieved at negligible costs to the mechanical properties of the final membranes. Therefore, due to the novel architecture of these copolymers that posses readily tailored compositions and are easily synthesized, the reported novel graft copolymer-based for the hydrophilization of intrinsically hydrophobic membranes has great potential for commercial applications.

Acknowledgements. We thank the National Natural Science Foundation of China (No. 20474068, 51173204), the Leading Talents Program of Guangdong Province, the Guangzhou Invited-Talents Special Project for Addressing Challenging Problems (NO 11D34060038), the Program for Comprehensive Strategic Cooperation between the Chinese Academy of Sciences and Guangdong Province (NO 2012B090400033), and the Program for Integration of Industry, Education and

Research in Guangdong Province (2011A091000007) for financial support. We also thank Dr. Ian Wyman for proofreading this paper.

References

1. S. Zhao, Z. Wang, Z. H. Qiao, X. Wei, C. X. Zhang, J. X. Wang and S. C. Wang, *J Mater Chem A*, 2013, **1**, 246-249.
2. Y. H. Zhao, K. H. Wee and R. B. Bai, *Acs Appl Mater Inter*, 2010, **2**, 203-211.
3. J. Schrier, *Acs Appl Mater Inter*, 2012, **4**, 3745-3752.
4. M. W. Lee, S. An, S. S. Latthe, C. Lee, S. Hong and S. S. Yoon, *Acs Appl Mater Inter*, 2013, **5**, 10597-10604.
5. Z. Liu, F. Luo, X. J. Ju, R. Xie, Y. M. Sun, W. Wang and L. Y. Chu, *J Mater Chem A*, 2013, **1**, 9659-9671.
6. L. R. Wang, H. Qin, S. Q. Nie, S. D. Sun, F. Ran and C. S. Zhao, *Acta Biomater*, 2013, **9**, 8851-8863.
7. L. Ma, H. Qin, C. Cheng, Y. Xia, C. He, C. X. Nie, L. R. Wang and C. S. Zhao, *J Mater Chem B*, 2014, **2**, 363-375.
8. J. G. Zhang, Z. W. Xu, W. Mai, C. Y. Min, B. M. Zhou, M. J. Shan, Y. L. Li, C. Y. Yang, Z. Wang and X. M. Qian, *J Mater Chem A*, 2013, **1**, 3101-3111.
9. H. Yamamura, K. Kimura and Y. Watanabe, *Environ Sci Technol*, 2007, **41**, 6789-6794.
10. J. H. Jiang, L. P. Zhu, L. J. Zhu, H. T. Zhang, B. K. Zhu and Y. Y. Xu, *Acs Appl Mater Inter*, 2013, **5**, 12895-12904.
11. H. Susanto, M. Balakrishnan and M. Ulbricht, *J Membrane Sci*, 2007, **288**, 157-167.
12. J. Y. Wang, Y. Y. Xu, L. P. Zhu, J. H. Li and B. K. Zhu, *Polymer*, 2008, **49**, 3256-3264.
13. J. Y. Park, M. H. Acar, A. Akthakul, W. Kuhlman and A. M. Mayes, *Biomaterials*, 2006, **27**, 856-865.
14. J. Zhu and G. Sun, *Acs Appl Mater Inter*, 2014, **6**, 925-932.
15. J. Zhao, F. S. Pan, P. Li, C. H. Zhao, Z. Y. Jiang, P. Zhang and X. Z. Cao, *Acs Appl Mater Inter*, 2013, **5**, 13275-13283.
16. J. Yuan, L. Tong, H. X. Yi, B. X. Wang, J. Shen and S. C. Lin, *Colloid Surface B*, 2013, **111**, 432-438.
17. H. Susanto and M. Ulbricht, *Water Res*, 2008, **42**, 2827-2835.

18. Y. H. Zhao, B. K. Zhu, L. Kong and Y. Y. Xu, *Langmuir*, 2007, **23**, 5779-5786.

19. D. M. He and M. Ulbricht, *J Mater Chem*, 2006, **16**, 1860-1868.

20. C. Cheng, L. Ma, D. F. Wu, J. Ren, W. F. Zhao, J. M. Xue, S. D. Sun and C. S. Zhao, *J Membrane Sci*, 2011, **378**, 369-381.

21. T. Luo, S. O. Lin, R. Xie, X. J. Ju, Z. Liu, W. Wang, C. L. Mou, C. S. Zhao, Q. M. Chen and L. Y. Chu, *J Membrane Sci*, 2014, **450**, 162-173.

22. J. Pieracci, J. V. Crivello and G. Belfort, *J Membrane Sci*, 2002, **202**, 1-16.

23. D. S. Wavhal and E. R. Fisher, *J Membrane Sci*, 2002, **209**, 255-269.

24. Y. Q. Wang, Y. L. Su, Q. Sun, X. L. Ma and Z. Y. Jiang, *J Membrane Sci*, 2006, **286**, 228-236.

25. A. M. S. de Jubera, J. H. Herbison, Y. Komaki, M. J. Plewa, J. S. Moore, D. G. Cahill and B. J. Marinas, *Environ Sci Technol*, 2013, **47**, 8642-8649.

26. J. S. Louie, I. Pinnau, I. Ciobanu, K. P. Ishida, A. Ng and M. Reinhard, *J Membrane Sci*, 2006, **280**, 762-770.

27. J. B. Qu, L. Y. Chu, M. Yang, R. Xie, L. Hu and W. M. Chen, *Adv Funct Mater*, 2006, **16**, 1865-1872.

28. L. Y. Chu, Y. Li, J. H. Zhu, H. D. Wang and Y. J. Liang, *J Control Release*, 2004, **97**, 43-53.

29. F. V. Adams, E. N. Nxumalo, R. W. M. Krause, E. M. V. Hoek and B. B. Mamba, *J Membrane Sci*, 2012, **405**, 291-299.

30. S. H. Choi, J. W. Chung, R. D. Priestley and S. Y. Kwak, *J Membrane Sci*, 2012, **409**, 75-81.

31. G. Arthanareeswaran, C. S. Latha, D. Mohan, M. Raajenthiren and K. Srinivasan, *Separ Sci Technol*, 2006, **41**, 2895-2912.

32. Z. F. Fan, Z. Wang, N. Sun, J. X. Wang and S. C. Wang, *J Membrane Sci*, 2008, **320**, 363-371.

33. J. F. Hester, P. Banerjee and A. M. Mayes, *Macromolecules*, 1999, **32**, 1643-1650.

34. P. Han, H. Yahui, W. Yang and L. Linlin, *J Membrane Sci*, 2006, **284**, 9-16.

35. H. Wu, J. Mansouri and V. Chen, *J Membrane Sci*, 2013, **433**, 135-151.

36. Y. Q. Zhang, P. Cui, T. D. Du, L. B. Shan and Y. L. Wang, *Sep Purif Technol*, 2009, **70**, 153-159.

37. E. Berndt and M. Ulbricht, *Polymer*, 2009, **50**, 5181-5191.

38. X. L. Ma, Y. L. Su, Q. Sun, Y. Q. Wang and Z. Y. Jiang, *J Membrane Sci*, 2007, **292**, 116-124.

39. B. Zornoza, S. Irusta, C. Tellez and J. Coronas, *Langmuir*, 2009, **25**, 5903-5909.

40. Y. L. Liu, C. H. Yu, L. C. Ma, G. C. Lin, H. A. Tsai and J. Y. Lai, *J Membrane Sci*, 2008, **311**, 243-250.

41. F. Y. Mahlicli and S. A. Altinkaya, *J Membrane Sci*, 2014, **449**, 27-37.

42. W. Wang, X. J. Huang, J. D. Cao, P. Lan and W. Wu, *Acta Biomater*, 2014, **10**, 234-243.

43. C. Dizman, M. A. Tasdelen and Y. Yagci, *Polym Int*, 2013, **62**, 991-1007.

44. T. A. Callaghan and D. R. Paul, *J Polym Sci Pol Phys*, 1994, **32**, 1847-1880.

45. T. Hasegawa, Y. Iwasaki and K. Ishihara, *Biomaterials*, 2001, **22**, 243-251.

46. Y. W. Chen, L. Ying, W. H. Yu, E. T. Kang and K. G. Neoh, *Macromolecules*, 2003, **36**, 9451-9457.

47. J. F. Hester, P. Banerjee, Y. Y. Won, A. Akthakul, M. H. Acar and A. M. Mayes, *Macromolecules*, 2002, **35**, 7652-7661.

48. Z. Yi, L. P. Zhu, L. Cheng, B. K. Zhu and Y. Y. Xu, *Polymer*, 2012, **53**, 350-358.

49. F. Liu, J. W. Hu, G. J. Liu, S. D. Lin, C. M. Hou, H. L. Zou, Y. Yang, Y. Wu and Y. M. Mo, *Polym Chem-Uk*, 2014, **5**, 1381-1392.

50. F. Liu, J. W. Hu, G. J. Liu, C. M. Hou, S. D. Lin, H. L. Zou, G. W. Zhang, J. P. Sun, H. S. Luo and Y. Y. Tu, *Macromolecules*, 2013, **46**, 2646-2657.

51. F. Liu, S. D. Lin, Z. Q. Zhang, J. W. Hu, G. J. Liu, Y. Y. TU, Y. Yang, H. L. Zou, Y. M. Mo and L. Miao, *Biomacromolecules*, 2014, **15**, 968-977.

52. C. M. Hou, J. W. Hu, G. J. Liu, J. D. Wang, F. Liu, H. Hu, G. W. Zhang, H. L. Zou, Y. Y. Tu and B. Liao, *Macromolecules*, 2013, **46**, 4053-4063.

53. T. Wu, P. Gong, I. Szleifer, P. Vlcek, V. Subr and J. Genzer, *Macromolecules*, 2007, **40**, 8756-8764.

54. D. X. Yin and M. Ulbricht, *J Mater Chem B*, 2013, **1**, 3209-3219.

55. C. Geismann and M. Ulbricht, *Macromol Chem Phys*, 2005, **206**, 268-281.

56. H. Yamanaka, Y. Teramoto and Y. Nishio, *Macromolecules*, 2013, **46**, 3074-3083.

57. Y. Zhang, M. G. Pan, C. Liu and J. L. Huang, *J Polym Sci Pol Chem*, 2008, **46**, 2624-2631.

58. G. Yilmaz, H. Toiserkani, D. O. Demirkol, S. Sakarya, S. Timur, Y. Yagci and L. Torun, *J Polym Sci Pol Chem*, 2011, **49**, 110-117.

59. G. J. Liu, Z. H. Lu and S. Duncan, *Macromolecules*, 2004, **37**, 4218-4226.

60. P. vandeWitte, P. J. Dijkstra, J. W. A. vandenBerg and J. Feijen, *J Membrane Sci*, 1996, **117**, 1-31.

61. H. C. Park, Y. P. Kim, H. Y. Kim and Y. S. Kang, *J Membrane Sci*, 1999, **156**, 169-178.

62. J. Y. Kim, H. K. Lee and S. C. Kim, *J Membrane Sci*, 1999, **163**, 159-166.

63. F. J. Tsai and J. M. Torkelson, *Macromolecules*, 1990, **23**, 775-784.

64. S. P. Nunes and T. Inoue, *J Membrane Sci*, 1996, **111**, 93-103.

TOC Graphic

Facbricaton of hydrophilic polysulfone membranes exhibited long-term stability via novel binary amphipilic graft copolymer-based approach.